Shock Tube Diagnostics Utilizing Laser Raman Scattering

Joseph W. Glaser* and Samuel Lederman†
Polytechnic Institute of New York, Farmingdale, New York

The application of the spontaneous laser Raman technique in the experimental analysis of temperature and specie concentration in an ionizing gas, using a high power Q-switched ruby laser, has been investigated. This technique is used as the diagnostic tool for the determination of flowfield conditions behind the reflected shock produced in a shock tube. Specie concentration and temperature of molecular nitrogen and singly ionized molecular nitrogen is obtained at hypersonic velocities. Comparison of the experimental data with theoretically derived results exhibits acceptable agreement for moderate temperatures behind the reflected shock. However, the significant data deviation from the mean also indicated that the experiment was operated near the limits of applicability for the spontaneous Raman technique. Other possible diagnostic techniques for use in this region are discussed.

I. Introduction

In recent years, the Aerodynamics Laboratory of the Polytechnic Institute of New York has been involved in the development and utilization of several light scattering techniques for use as diagnostic tools in flowfield analysis. Typically, these experiments involved the determination of concentrations of major components of the flowfield and their temperatures. Results of these experiments have been documented in numerous journals by the Aerodynamics Laboratory and other laboratories (Refs. 1-5, for example). It has become apparent that a single diagnostic technique will not yield optimal results in all flowfield situations. For example, environments that are inherently noisy may exhibit an unacceptably low signal to noise ratio when using spontaneous Raman scattering to obtain flowfield information. In such a situation, diagnostic methods that have a large scattering cross section, such as coherent anti-Stokes scattering (CARS[3]), would probably yield data that could be analyzed more easily.

Additional problems are encountered when the flowfield being analyzed is undergoing chemical reactions. A wide assortment of difficulties arise depending on the type of flowfield involved; specifically, whether the flowfield is an external (such as exhaust flows) or an internal (e.g., combustion chamber) one. While hardly trivial, the diagnostics of the external combustion flowfield does allow almost unlimited optical accessibility. Internal combustion diagnostics present problems of accessibility, as well as modifications of the internal field necessary to introduce the beam into the flowfield. These disturbances must be minimized. Since it is single ended,[1] Raman scattering requires the fewest modifications of the physical structure.

During the last thirty years, the shock tube has become an important research tool for studying processes in high temperature gases and fast gas flow. In this device, a shock wave produced as a result of the sudden bursting of a diaphragm separating a region of high pressure from one at low pressure, creates a region of high temperature and pressure.[6] Since the thermochemical state of high density gas is known, the shock tube becomes a valuable tool for calibrating Raman measurement apparatus and validating Raman theory at elevated temperature conditions. These features prompted White[7] to suggest the use of Raman scattering for pointwise measurement of vibrational and/or rotational temperatures behind the incident shock wave. From his own work, he was able to determine specie concentration of various components during methane oxidation, regardless of whether or not thermochemical equilibrium existed. Boiarski[8] attempted to observe Raman scattering from high-temperature oxygen and nitrogen behind an incident shock wave in air. He determined postshock temperature and density conditions using laser Raman and compared these to available shock tube data. This data was part of a calibration procedure of experimental equipment for use in gasdynamics laser cavity diagnostics.

This study utilizes laser Raman scattering as the diagnostic technique in the determination of density and temperature behind the reflected shock in a shock tube. The device is used to obtain ionized flows which are studied using the spontaneous Raman effect. This is of importance in the characterization of MHD flows and some combustion chamber processes, particularly since the technique is pointwise remote and nonintrusive. Since the Raman shift for each Raman active specie is different, it is possible to obtain temperature and specie information for each specie of interest. Thus, it theoretically is possible to obtain temperature and specie concentration information about an entire flowfield instantaneously, simultaneously, and remotely. The experimentally determined data were then compared with theoretically derived values. The objective of the study was the extension of spontaneous Raman measurements to high-temperature regions that are to be found in some energy generation devices and to determine the limits of applicability at these elevated temperatures.

II. Theory

A. Raman Effect

Raman scattering theory has been well documented in numerous references (for example, Refs. 9 and 10). This phenomenon occurs when significant amounts of energy are exchanged between incident light photons and the internal states of a molecule subjected to this incident radiation. Not all transitions are allowed, but are governed by specific selection rules. When these rules are applied, it can be shown that there arise three possible branches due to the rotational transitions accompanying the vibrational scattering process. Of these, the so called Q branch is the strongest; comprising approximately 98% of the total intensity.[9] It was this branch that was used in the determination of temperature and specie

Received Sept. 8, 1981; revision received May 11, 1982.

*Graduate Research Assistant; presently Senior Research Associate, Science and Technology Laboratory, International Harvester. Member AIAA.

†Professor, Mechanical and Aerospace Engineering. Member AIAA.

concentration. To utilize this branch for diagnostic purposes, its intensity, spectral distribution, and position must be considered. This is obtained in a manner similar to that discussed by Lederman[1] and Lapp et al.[2] By use of the system of equations described therein, it is possible to determine theoretically the intensity of the Raman band of a particular specie under given temperature conditions. This can be done regardless of whether equilibrium or nonequilibrium conditions exist. The latter situation occurs in the case of real flows subject to large temperature gradients, since the rotational degrees of freedom reach equilibrium much more rapidly than the vibrational degrees of freedom. Figure 1 displays the results of a calculation involving molecular nitrogen at various temperatures for both equilibrium and nonequilibrium conditions, assuming a triangular slit function of 1 Å. Note the decrease and shift of the peak intensity as temperature is increased. If narrow bandpass filters are used, it is quite conceivable for the peak Raman wavelength to lie outside the filter bandpass. This will be discussed in more detail in the results section.

The observed Raman intensity flux is dependent upon several factors. These include the energy of the incident radiation E_0, the molecular number density N, scattering cross section σ, optically observed path length of the laser ℓ, optical collection angle Ω, optical efficiency ϵ, detector efficiency η, and the energy per photon E_p. In the measurement of density, the ratio $E_0\sigma\ell\,\Omega\epsilon\eta/E_p=K$ is a constant to be determined by calibration at known density. Then, the number of scattered photons n_s is measured and the molecular number density N is calculated using

$$N=n_s/K \tag{1}$$

Note that in the presence of background noise, the total signal will be the sum of the desired count n_s and the background count n_b. This noise signal must be accounted for. The next section describes how this was done.

There are several experimental factors influencing Eq. (1). Specifically, these are the observation length and collection solid angle, ℓ and Ω, respectively. Since Raman scattering is nearly isotropic, an increased collection angle implies greater collection efficiency. Similarly, the scattering volume as determined from the incident beam cross-sectional dimension and optical field of view varies linearly with the square of the beam diameter and beam length. This aspect indicates the pointwise ability of Raman scattering. Therefore, by focusing the incident beam and using optical stops to obtain a small observed length, the spatial resolution will be improved—but at the expense of signal intensity.

The technique used to calculate the temperature involves finding the ratio of the intensities of the Stokes and anti-Stokes components and utilizing the Boltzmann distribution to determine the number of molecules in each vibrational

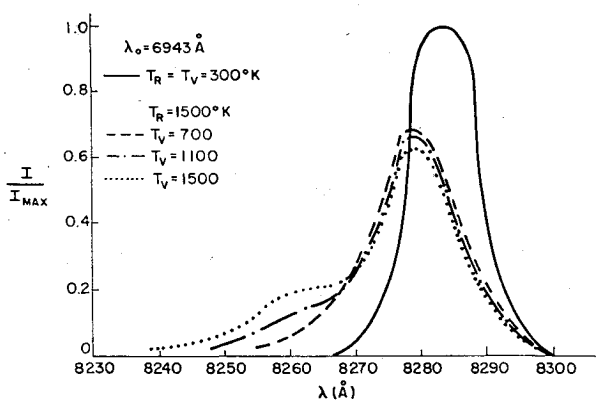

Fig. 1 Intensity variation of nitrogen Stokes band for equilibrium and nonequilibrium conditions.

state. Then,

$$T=\frac{hc}{k}\,\frac{\nu}{In(I_s/I_a)+4\ell n(\nu_0+\nu)/(\nu_0-\nu)} \tag{2}$$

where I_s and I_a are the intensities of the Stokes and anti-Stokes Q branch, respectively.

There is a direct relationship between increases in temperature and increases in the intensity of the anti-Stokes signal. Caution must be exercised when evaluating the number density since the Raman line intensities are dependent simultaneously upon temperature and number density.[1] Since both the Stokes and anti-Stokes components will be present, measurement of the intensity of either component can be used to determine the concentration of a particular specie, when the temperature dependence is taken into account. For the cae where the incident radiation is polarized vertically and the entire vibration-rotation Raman band is observed, the intensity of the scattered radiation for an individual specie becomes[1]

$$I_{s,a}=\frac{K(\nu_0\pm\nu)^4NI_0}{1-\exp(-hc\nu/kT)} \tag{3}$$

Equation (3) gives the functional dependence of the scattered intensity upon the various governing independent parameters. Note that the scattered intensity varies linearly with number density.

B. Shock Tube Theory

The shock tube is essentially a device in which a plane shock wave is produced by the sudden bursting of a diaphragm that separates a high-pressure low molecular weight gas from a test gas at lower pressure. Behind the shock wave the experimental gas is brought almost instantly to a known and controlled high temperature, and may be held at steady temperature and pressure for a few hundred microseconds (depending on a number of parameters). Since the density of the gas behind the wave is relatively large, this will result in an increased Raman signal. A further increase in the thermodynamic properties of the gas is accomplished upon shock reflection from the end wall of the shock tube. It was this region that was analyzed during the course of this experiment. Derivation of these equations as well as discussions concerning the different types of shock tubes can be found in Refs. 6 and 14.

Since thermodynamic conditions in the shock tube change as the different wave fronts move past a given point, the observation time becomes an important parameter. This is the time a given set of thermodynamic conditions exist. Behind the reflected shock it is defined as the time between incident shock reflection with the end wall and its collision with the contact surface. If $M_1^2\gg 1$, i.e., a strong shock and a perfect gas is assumed, then the observation time is given by

$$\Delta t=\frac{X_1}{M_1a_1}\,\frac{\gamma-1}{2\gamma} \tag{4}$$

with a 5% error at $M_1=5$ and where X_1 is the length of the shock tube driven section, with the subscript *1* signifying conditions in the driven section before shock arrival.

In real flows, however, a velocity gradient normal to the flow and close to the walls of the tube gives rise to a layer of gas across which the flow will be retarded—the boundary layer.[12] The removal of gas from the shock wave by the boundary layer results in an acceleration of the contact surface toward the shock front, decreasing observation time behind the incident shock, which affects the observation time behind the reflected shock.

The growth of the boundary layer behind the incident shock has a minimal effect on the shock front since the boundary layer vanishes at that point. Only the pressure waves

propagating in the flow behind the shock are responsible for any deviations. However, after the shock has reflected from the wall, it must pass through the boundary layer. This interaction results in a complicated flow pattern that has been theoretically analyzed by Mark[13] and Rudinger.[14] Their analyses have been tested experimentally by numerous researchers. Johnson and Britton[15] noted that real gas effects were the predominant factors influencing the flow immediately behind the reflected shock. For data taken later in time, viscous effects began to become important. They found that density as well as pressure measurements agreed well with theory immediately behind the reflected shock. However, these data did not remain constant with time but showed a definite increase, indicating that the gas behind the reflected shock was not stationary as ideal theory predicts, but is in motion. Temperature, obtained indirectly from the experimentally derived density and pressure data was found to be lower than the calculated value by approximately 4% at Mach numbers on the order of 2. This difference was found to decrease as the incident Mach number was increased.

A possible explanation for the behavior of the gas behind the reflected shock was proposed by Rudinger.[14] It was his contention that since the flow velocity at the wall must be zero, the deceleration of the gas near the wall would be accomplished by weak adiabatic compression waves following the shock. On the basis of this theory, the temperature adjacent to the wall will be within 50° of the temperatures calculated from the incident velocities. Therefore, the calculated reflected temperatures at the end wall are, in fact, more reliable than the anomalous behavior suggested. Although compression waves of this sort cannot be detected, pressure measurements behind the reflected shock have confirmed calculations based on ideal theory. For data taken in the central core of a gas very close to the end wall of a tube having a low length to diameter ratio, Glass and Martin[16] found these effects to be minimal. It was this region that was analyzed experimentally. The method used is detailed in the next section.

III. Experimental Procedure

A double diaphragm shock tube with a converging nozzle connecting the driver to driven sections was used in this experiment (Fig. 2). Two perpendicular grooves of known depth were machined onto the copper disks, making it possible to determine approximately the differential pressure at which the diaphragms would rupture. If the entire driver section is pressurized to 0.75 times this pressure, and the valve separating the short driver section from the longer one is closed, the longer section may be pressured to twice the short section pressure (see Fig. 2). Releasing the pressure in the shorter section subsequently causes the diaphragms to burst, starting with the one separating the long from the shorter driver section. Non-one-dimensional flow deviations are modified by this double diaphragm arrangement and by the converging nozzle connecting the driver to driven sections.[6] The driver gas was hydrogen and air was used as the driven gas. In order to generate the temperature and density conditions necessary for this study, the driver gas pressure was varied between 6.206-8.274 MPa, while the driven gas pressure was varied between 1 and 20 Torr.

Shock velocities were determined by measuring the time it took the pressure wave to travel between two transducers mounted a known distance apart. A total of three pressure transducers were used in this experiment. Two transducers mounted upstream of the end wall measured incident shock pressures, while the third, located at the end wall, monitored reflected shock pressures. It was, therefore, possible to compute shock velocities between these three transducers, and from this information, determine the degree of shock wave attenuation from the decrease in shock speed. By comparing the results of the three transducers it was found that the shock speed attenuation was negligible (on the order of 1% at $M = 12.59$).

The Raman chamber, located at the end of the shock tube, contained three windows to allow optical access for use in the reflected shock diagnostics. A window parallel to the incoming shock was used to allow the incident laser beam to pass into the shock tube. Two windows perpendicular to the incoming shock were used to collect the scattered Raman signals.

Signal intensity is directly affected by several experimental factors as indicated by Eq. (1). Specifically, these depend upon the size of the optical windows, focal length, and the required spatial resolution. Since the windows are centered with respect to the shock tube and the shock wave is assumed planar, the entire planar field of light is collected. This significantly increases the signal intensity without appreciably increasing the noise.

Consequently, the optical system used to collect the scattered light is much simpler than that used in the past.[5] Only a

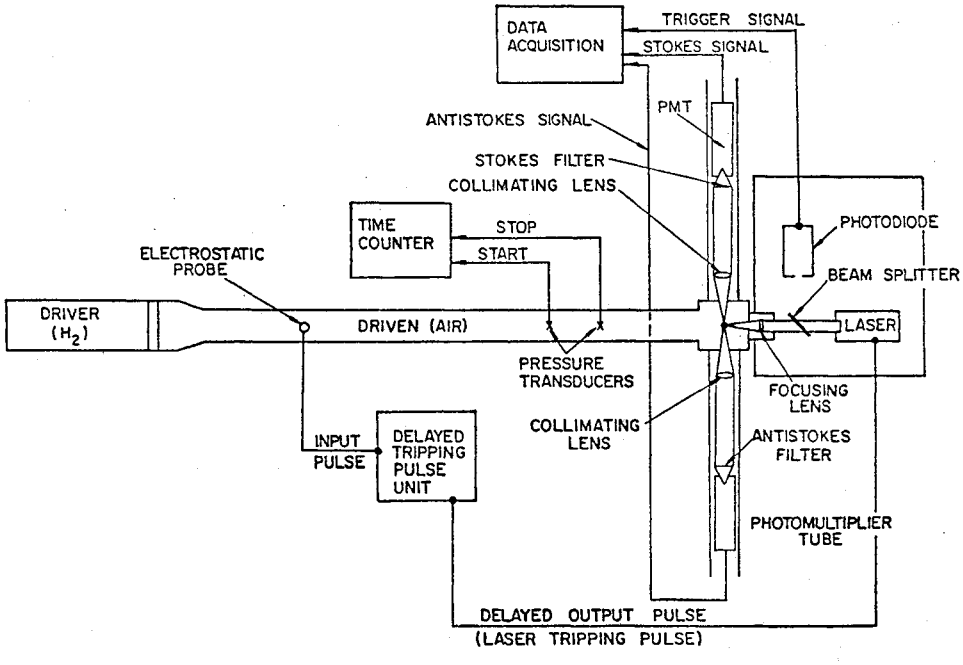

Fig. 2 Schematic diagram of the shock tube experiment.

single collimating lens in series with a filter is required. Each filtering system consisted of a Stokes or anti-Stokes pass filter in series with a Rayleigh reject filter. Thus, only the particular line of interest would be transmitted. The filters were placed in front of an RCA8853 photomultiplier tube.

In order to determine the relative intensities of the noise signals, the laser was fired into the shock tube under various nonshock conditions. Background due to surface scattering was determined by firing the laser into an evacuated shock tube. Similarly, the intensity of the unrejected Rayleigh scattered light was found by pressurizing the shock tube with carbon dioxide whose Raman lines are far from the N_2^+ lines. These background noise signals were then subtracted from the total signal obtained during a test. This procedure was repeated after each test since background noise increased due to copper particle deposit on the windows. Periodically, the shock tube had to be disassembled and cleaned of these particles. In addition, since a gas compressed to a high temperature and pressure will emit radiation, the emission spectrum of the shocked gas had to be determined and these signals subtracted from the Raman data signals. This was accomplished by firing the shock tube and collecting and analyzing the emitted radiation in a spectrometer. The resultant spectrum, at a Mach number of 9.5, is shown in Fig. 3.

A TRG model 104A Q-switched ruby laser system was used as the light source in this experiment. It was an air cooled laser capable of delivering 1.5 J in 15 ns at 694.3 nm at a rate of one pulse every 3 min. Although slow by present standards, the cycle time was not an important factor since it took at least that long to prepare for each test.

To ascertain the coincidence of the laser pulse and the reflected shock arrival, a timing analysis had to be performed. Q switching delays the onset of the laser pulse by causing the energy to be stored, resulting in a high-power pulse being emitted over a short (approximately 15 ns for this laser) period of time. The delay time is set to optimize the output energy. This delay time was found to be less than the time required for the shock wave to reach the end wall. To account for this, a signal delay to fire the laser was incorporated into the system.

Scattered light signals were collected normal to the incident beam as shown in Fig. 2. The resultant signal was processed by a PDP-8E minicomputer. These signals are of the same duration as the laser pulse, 15 ns. In order to perform the analog to digital conversion, the PDP-8E minicomputer requires an analog signal of at least 30 μs. Since this was not the case, the photomultiplier tube signal had to be fed into a Chronetics model 166 linear gate with a stretch and hold module which expanded the signal to the required length while leaving the amplitude unaffected.

A gate generator was used which allowed data to be obtained only when the laser was fired. Thus, the signal monitored by the computer resulted only from the Raman scattered light signal. Data was obtained from a photo diode, which monitored laser intensity and photomultiplier tubes from whence the Stokes and anti-Stokes intensities were obtained. The laser intensity was monitored so that variations in scattered signals due to laser variations could be accounted for. The data acquisition and processing system have been previously described (see, for example, Refs. 1, 4, and 5).

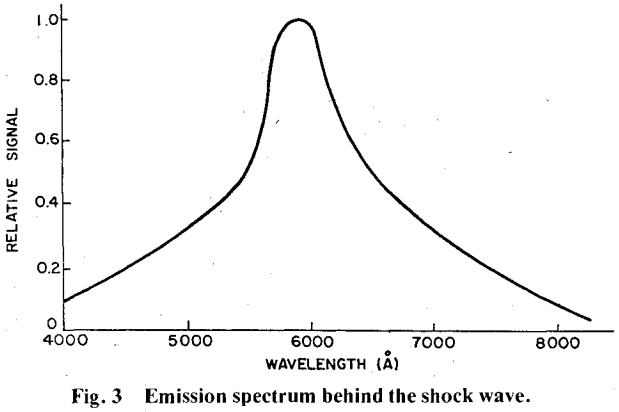

Fig. 3 Emission spectrum behind the shock wave.

IV. Experimental Results and Discussion

This experiment was concerned primarily with the use of laser Raman diagnostics for the determination of temperature and concentration of molecular and singly ionized nitrogen behind the reflected shock. Since this latter specie is not abundant at room temperature and is barely observable even at the temperatures used in this experiment, it is important to determine the significance of the energy introduced into the gas by the laser beam. The wavelength of the incident radiation was 694.3 nm which corresponds to an energy per photon of $E=hc/\lambda=1.79$ eV where $hc=12{,}400$ eV-A. Utterback[17] determined the ionization potential of the N_2 molecule-molecule collision process to be 15.6 eV. Similarly, the atom-atom collision process producing N_2 requires an

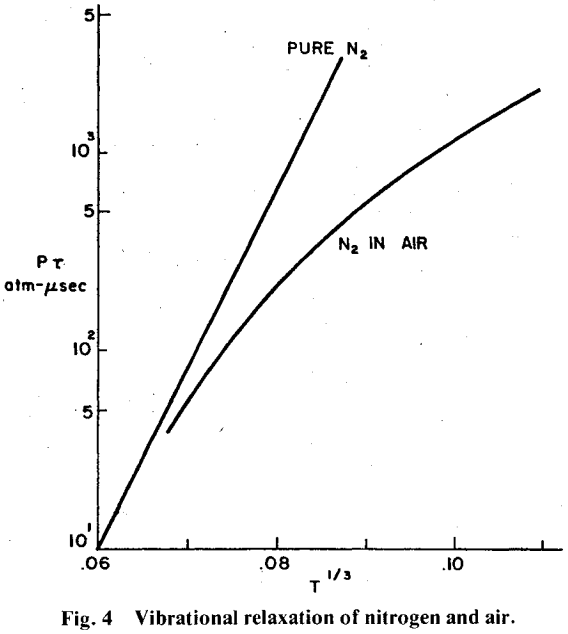

Fig. 4 Vibrational relaxation of nitrogen and air.

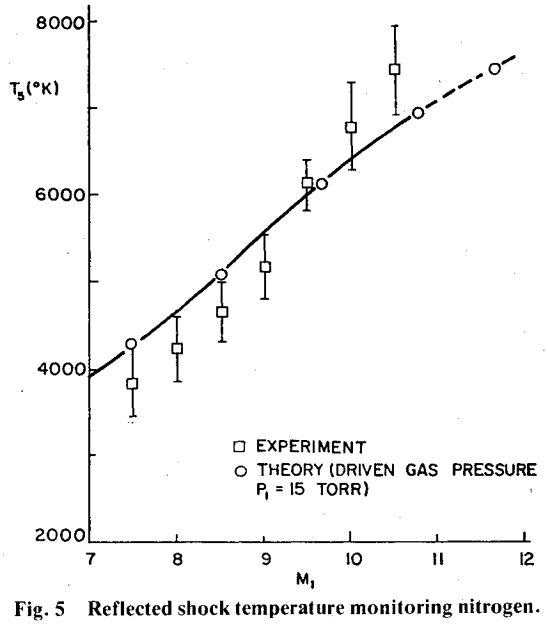

Fig. 5 Reflected shock temperature monitoring nitrogen.

energy input of 5.8 eV. Therefore, the energy introduced into the system due to photon-molecule interaction is assumed to have a negligible effect on the production of the ionized specie.

From this information, excitation studies on air and air-like mixtures were undertaken (for example, Ref. 18). These studies were concerned primarily with reaction rates and relaxation times of the various components. By monitoring electron density, Teare[19] concluded that conditions behind the shock have stabilized after the shock has moved about 10 cm further downstream at $M=10$. This corresponds to a time after shock passage of approximately 30 μs. This delay time is due mainly to the long relaxation time of the nitrogen molecule, as pointed out by Millikan and White.[18] They also observed that as the temperature behind the shock was increased, relaxation times decreased. A compilation of some of these results is presented in Fig. 4.

From the preceding it is seen that there exists a region behind the shock in which nonequilibrium conditions exist. Since the results obtained from the experimental procedure assume equilibrium conditions to prevail, data cannot be taken in the region immediately behind the shock wave. Thus, the minimum time prior to which data cannot be taken was determined to be 3 μs.

Using Eq. (4), the computed total observation time at Mach 10 is 110 μs. This equation, however, neglects real gas effects which tend to reduce the ideal observation time.[6] Incorporating these effects results in an observation time of approximately 75 μs. Data taken after this time were found to exhibit unfavorable signal to noise ratios. From the given limits, it was established that optimal signal to noise ratios were obtained for data taken between 5-30 μs after shock passage.

Under these temporal limitations, data using the experimental arrangements of Fig. 2 was collected. The Stokes and anti-Stokes signals were used to determine temperature and concentration of N_2 and N_2^+ behind the reflected shock. Concentration measurements were obtained using the anti-Stokes signals, since, at the temperature expected, they are more intense than the Stokes signal. Equations (2) and (3) were used for the determination of temperature and concentration, respectively. Data for N_2 are presented in Figs. 5 and 6 for temperature and concentration with respect to Mach number. Figures 7 and 8 display the results for N_2^+. Theoretically derived data, which are also plotted on these curves, were obtained from a program which was first verified by comparison to results obtained in Refs. 20 and 21.

Because of the high background noise level, it became progressively more difficult to obtain reliable data at low concentrations. This was true because the degree of ionization decreases as the Mach number and, hence, the temperature. As can be seen in Figs. 7 and 8, experimentally determined N_2^+ data exhibit a high degree of scatter, particularly at the lower Mach numbers. This is in contrast to the molecular nitrogen data displayed in Figs. 5 and 6, since at the temperatures considered here significant amounts of molecular nitrogen still exist.

Another source of error can best be described by referring to Fig. 1. This figure illustrates the effects of increasing temperature on the Raman spectrum, specifically the N_2 Stokes spectrum. Note that as the temperature is increased, the higher level vibrational-rotational energy levels are excited. The peak intensities decrease and the entire spectrum broadens significantly as temperature is increased.

Two problems associated with the technique described in Sec. III become apparent. The use of narrow bandpass filters results in the rejection of a significant portion of the Raman scattered signal at elevated temperatures (above 2000 K). Furthermore, as temperature is increased, the peak signal shifts toward the shorter wavelength. When very narrow filters (FWHM <5 Å) are used, the consequence of this wavelength shift is even weaker signal intensities, leading to still lower signal to noise ratios.

In order to compensate for this effect, a detailed analysis of the filter transmission vs wavelength was done. From this, a weighting function was found which was used to normalize the experimentally determined signal. It was found that the normalized Stokes signal increased from those values derived when a less sophisticated normalization procedure was used. The increased Stokes signal resulted in a decreased temperature from that reported earlier.[5] Note also that since filter characteristics have a tendency to change with time, the transmission spectrum was periodically analyzed. During the course of this experiment, these characteristics remained stable, so no adjustments to the normalization function were required.

The aforementioned wavelength broadening leads to a second drawback on the use of this technique at these elevated temperatures; that is, the spectral interference of the rotational wings from different species. At the Stokes level,

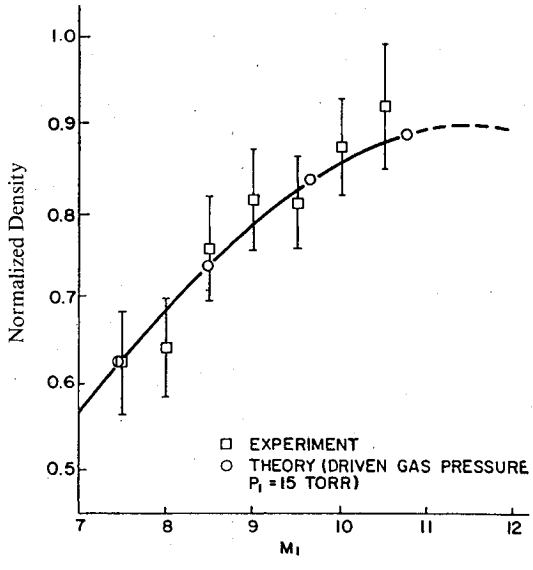

Fig. 6 Normalized nitrogen concentration behind the reflected shock.

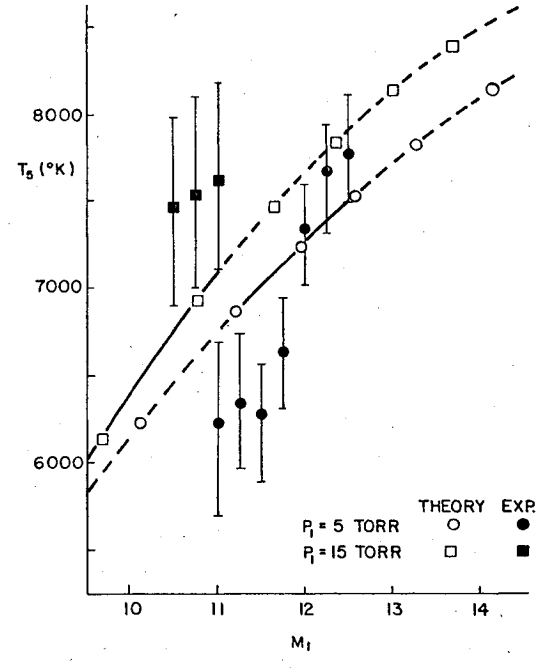

Fig. 7 Reflected shock temperature monitoring singly ionized molecular nitrogen.

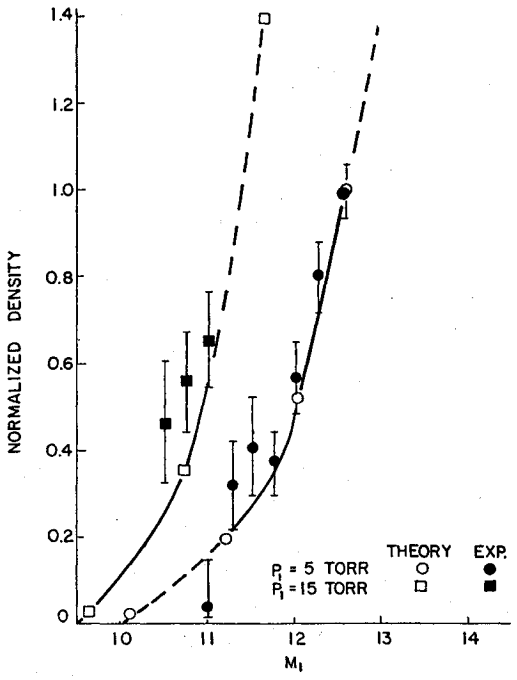

Fig. 8 Normalized singly ionized molecular nitrogen concentration behind the reflected shock.

the N_2^+ line at room temperature would appear at 8153 Å. From Fig. 1, note that at room temperature the peak N_2 Raman stokes signal intensity occurs at 8283 Å. At this temperature, for wavelengths smaller than 8272 Å, the rotational wings do not add appreciably to the total energy of the spectrum. As the temperature is increased, the peak Raman Stokes signal intensity will shift toward the shorter wavelengths. In addition, at these temperatures, the rotational wings broaden and can affect the Raman signal emanating from the N_2^+ ion. Since both of these signals are at the same wavelength, it would become increasingly difficult to experimentally determine their respective contributions to the total signal strength.

V. Conclusions

It has been shown that the spontaneous Raman effect may be used in the determination of temperature and specie concentration in an ionized gas. This has particular applicability in the study of magnetohydrodynamic flows, since, as with other optical techniques, Raman scattering is pointwise remote and nonintrusive. Additionally, the Raman scattered signal is linearly dependent upon the specie number density. Since the Raman signal is specific it is possible to monitor a number of different species simultaneously. This is perhaps its single most powerful feature. However, as a result of its low scattering cross section, signal intensities will also be small. In the analysis of environments which possess high background radiation, the signal to noise ratio can, therefore, become unacceptably low.

The effect of high temperatures is to affect spectral broadening and to reduce peak intensities of the Raman band. The former effect can result in spectral band interference from intersecting Raman spectra due to different species. Signal intensities are then equal to the sum of the various interfering lines which cannot be separated experimentally. Erroneous results, therefore would be obtained if the various lines were of nearly equal intensities. Narrow bandpass filters would further reject a large percentage of the actual Raman signal due to signal broadening. These problems impose definite restrictions on the applicability of spontaneous Raman scattering at highly elevated temperatures.

Care also must be exercised that all sources of background noise be accounted for and that these effects be minimized. Hostile environments impose the additional restriction that the background conditions may change with time. This situation must be monitored and appropriately compensated for.

Results using spontaneous Raman scattering have been obtained in a shock tube in the region behind the reflected shock. All the problems just listed have been acknowledged and minimized to the extent possible. However, as can be seen from Figs. 5-8, the deviation of the data from the mean is very high. This indicates that for the conditions encountered in this experiment, behind the reflected shock, limits of applicability for the use of the spontaneous Raman scattering technique are being approached. This is found to be the case even for N_2 whose concentration is relatively high (Fig. 6). For these conditions then, it may be advisable to use enhanced Raman techniques such as coherent anti-Stokes Raman scattering (CARS).

Acknowledgment

This paper was taken from the dissertation submitted to the Faculty of the Polytechnic Institute of New York in partial fulfillment of the requirements for the degree Doctor of Philosophy (Aeronautics and Astronautics) June 1982.

References

[1] Lederman, S., "The Use of Laser Raman Diagnostics in Flow Fields and Combustion," *Journal of Progress in Energy Combustion Science*, Vol. 3, Jan. 1977, pp. 1-34.

[2] Lapp, M., Penny, C.M., and Asher, J.A., "Applications of Light Scattering Techniques for Measurement of Density, Temperature, and Velocity in Gas Dynamics," 73-0045, April, 1973.

[3] Regnier, P., Moya, F., and Taran, J.P.E., "Gas Concentration Measurement by Coherent anti-Stokes Scattering," *AIAA Journal*, Vol. 12, June 1974, pp. 826-831.

[4] Lederman, S., "Developments in Laser Based Diagnostic Techniques," *Twelfth International Symposium on Shock Tubes and Waves*, Magnes Press, Jerusalem, 1980, pp. 48-65.

[5] Lederman, S., Celentano, A., and Glaser, J., "Temperature, Concentration, and Velocity in Jets, Flames, and Shock Tubes," *Physics of Fluids*, Vol. 22, June 1979, pp. 1065-1072.

[6] Glass, I.I. and Hall, J.G., "Shock Tubes," NAVORD Rept. 1488, Vol. 6, No. 95, 1959.

[7] White, D.R., "Shock Tube Studies of Nitrogen Vibrational Relaxation and Methane Oxidation," Aerospace Research Laboratory Report, ARL 70-0107, June 1970.

[8] Bioarski, A.A., "Shock Tube Diagnostics Utilizing Laser Raman Spectroscopy," Naval Surface Weapons Center Report, NSWC/WOL/TR75-53, June 1975.

[9] Herzberg, G., *Molecular Spectra and Molecular Structures: II Infrared and Raman Spectra*, Van Nostrand, 1947.

[10] Placzek, G., "The Rayleigh and Raman Scattering," Translation Series, University of California-Livermore, UCRL-TRANS-526 (1), March 1959.

[11] Liepmann, H.W. and Roshko, A., *Elements of Gasdynamics*, J. Wiley & Sons, Inc., New York, 1957.

[12] Crocco, L., "Considerations on the Shock-Boundary Layer Interaction," *Proceedings of the Conference on High Speed Aeronautics*, Polytechnic Institute of Brooklyn, Jan. 1955, pp. 75-112.

[13] Mark, H., "The Interaction of a Reflected Shock Wave with the Boundary Layer in a Shock Tube," *Journal of Aerospace Sciences*, Vol. 24, Feb. 1957, p. 304.

[14] Rudinger, G., "Effects of Boundary Layer Growth in a Shock Tube on Shock Reflection from a Closed End," *Physics of Fluids*, Vol. 4, No. 12, 1963, pp. 1463-1473.

[15] Johnson, C.D. and Britton, D., "Shock Waves in Chemical Kinetics: The Use of Reflected Shock Waves," *Journal of Chemical Physics*, Vol. 38, April 1963, pp. 1455-1462.

[16] Glass, I.I. and Martin, W.A., "Experimental and Theoretical Aspects of Shock Wave Attenuation," *Journal of Applied Physics*, Vol. 26, January 1955, p. 113.

[17] Utterback, N.G., "Ionization of Nitrogen Molecules by Nitrogen and Oxygen Molecules," *Physics Review*, Vol. 129, No. 1, 1963, pp. 219-224.

[18] Millikan, R.C. and White, D.R., "Systematics of Vibrational Relaxation," *Journal of Chemical Physics*, Vol. 39, Dec. 1963, p. 3209.

[19] Teare, J.D., "Ionization Behind Shock Waves," *Ionization in High Temperature Gases*, edited by K.E. Shuler, Academic Press, New York, 1963, pp. 217-283.

[20] Menard, W.A. and Horton, T.E., "Shock Tube Thermochemistry Tables for High Temperature Gases, Vol. I, Air," Jet Propulsion Laboratory, Pasadena, Calif., Rept. 32-1408, Nov. 1969.

[21] Glaser, J.W., "Shock Tube Diagnostics Utilizing Laser Raman Scattering," Ph.D. Thesis, Polytechnic Institute of New York, June 1982.